Catalysis Science & Technology

ROYAL SOCIETY OF CHEMISTRY

PAPER

View Article Online
View Journal | View Issue

Check for updates

Cite this: *Catal. Sci. Technol.*, 2026, **16**, 980

Impact of impurities in covalent organic frameworks on catalytic properties of supported isolated Pd complexes

Ruby Dane Deeter, †[a] Hridita Purba Saha, †[b] Ayman M. Karim *[b] and Hani M. El-Kaderi *[a]

Supported single-atom catalysts (SACs) have garnered significant interest due to their distinct electronic and geometric properties compared to metal nanoparticles. Covalent organic frameworks (COFs), owing to their high surface area and tunable functionalities, serve as promising supports for stabilizing isolated metal atoms. In this work, we synthesized a $PdCl_2$-functionalized pyrene-based COF ($PdCl_2$@Py-1P COF) that offers uniform binding sites ideal for immobilizing Pd single atoms. However, the synthetic route for pristine Py-1P COF could incorporate Pd impurities during synthesis, resulting from the incomplete removal of the homogeneous $Pd(PPh_3)_4$ catalyst used in the synthesis of the 1,3,6,8-tetrakis(4-aminophenyl)pyrene (PyTTA) monomer *via* Suzuki–Miyaura cross-coupling reaction. To our knowledge, no study has been reported on the role of Pd impurities in pristine COFs, complicating the distinction between the activity of Pd single atoms and the pristine COF itself. To address this, we used a combination of X-ray photoelectron spectroscopy (XPS), and CO-DRIFTS (diffuse reflectance infrared Fourier transform spectroscopy) to systematically investigate different purification strategies to minimize the impact of Pd impurities on ethylene hydrogenation kinetics. The $PdCl_2$ complexes deposited on the COF ($PdCl_2$@Py-1P COF) were isolated and structurally uniform. However, the Pd impurities in the pristine COF exhibit significant activity for ethylene hydrogenation, masking the activity of $PdCl_2$@Py-1P COF. To minimize Pd carryover, the PyTTA monomer was purified prior to COF synthesis by triphenylphosphine (PPh_3) treatment or acid, lowering the Pd content in the resulting COFs from 0.35 wt% (untreated) to 0.23 wt% (PPh_3) and 0.04 wt% (acid). Acid purification removed the vast majority of Pd impurities from the pristine (pre-deposition) COF, thereby enabling measurement of the intrinsic kinetics of subsequently deposited $PdCl_2$ complexes. The results emphasize the importance of the monomer purification process to accurately measure the intrinsic properties of Pd single atoms within the COF structure.

Received 3rd October 2025,
Accepted 16th December 2025

DOI: 10.1039/d5cy01181g

rsc.li/catalysis

Open Access Article. Published on 16 December 2025. Downloaded on 2/14/2026 6:47:07 PM.
This article is licensed under a Creative Commons Attribution-NonCommercial 3.0 Unported Licence.

Introduction

Supported metal nanostructures are widely employed heterogeneous catalysts in industrial applications, with metal particle size being a critical factor influencing catalytic behavior. The smallest and most efficient form of these catalysts is what is referred to as a single-atom catalyst (SAC), in which individual metal atoms are atomically dispersed on a support. SACs offer exceptional atom utilization—particularly beneficial for noble metals—and have demonstrated high catalytic activity and selectivity for some reactions due to their unique electronic properties.[1] Palladium is especially important in catalysis, playing a central role in selective hydrogenation,[2–5] dehydrogenation,[6–9] and cross-coupling reactions.[10–13] Consequently, numerous synthetic strategies have been developed to control the nuclearity of Pd species. Unlike Pd nanoparticles, which often favor over-hydrogenation due to the presence of extended metal ensembles, atomically dispersed Pd supported on oxides or carbonaceous materials exhibits significantly enhanced selectivity toward ethylene, even under ethylene-rich conditions.[14] For instance, Pei *et al.* reported a Cu-alloyed Pd single-atom catalyst with high ethylene selectivity (~85%) at complete acetylene conversion.[15] Similarly, Yan *et al.* synthesized atomically dispersed Pd on graphene *via* atomic layer deposition, achieving 100% selectivity toward butene at 95% conversion in the selective hydrogenation of 1,3-butadiene.[16]

Among the emerging novel supports for SACs are covalent organic frameworks (COFs). COFs are crystalline, highly

[a] *Department of Chemistry, Virginia Commonwealth University, Richmond, Virginia 23284-2006, USA. E-mail: helkaderi@vcu.edu*
[b] *Department of Chemical Engineering, University of Virginia, Charlottesville, VA 22901, USA. E-mail: pqg9zx@virginia.edu*
† Authors contributed equally.

This journal is © The Royal Society of Chemistry 2026

Open Access Article. Published on 16 December 2025. Downloaded on 2/14/2026 6:47:07 PM. This article is licensed under a Creative Commons Attribution-NonCommercial 3.0 Unported Licence.

porous, extended two- and three-dimensional organic frameworks constructed by linking organic building units using covalent bonds. The reticular synthetic approach of COFs enables high surface area and controlled pore size, shape, and chemical functionality, rendering COFs ideal platforms for a broad range of applications[17,18] such as gas capture/separation, heterogeneous catalysis, energy storage, sensors, and medical uses. For catalytic applications, the high surface area and chemical functionality of the pores are crucial for stabilizing both metal nanoparticles and SACs.[19] Wang *et al.* first demonstrated the catalytic application of COFs by preparing Pd/COF-LZU1 *via* post-metalation for Suzuki–Miyaura coupling reaction.[20] COFs have also been demonstrated as effective supports for nanoparticles and single atoms of metals like platinum,[21] rhodium,[22] ruthenium,[23] iridium,[24] copper,[25] cobalt,[26] and palladium[27] for catalytic purposes. For instance, we have reported the synthesis of $PdCl_2$@ILCOF-1 (imine-linked COF) and demonstrated its application in gas-phase ethylene hydrogenation.[28] The high surface area and abundant imine-sites allowed for high palladium loading (~18 wt%) and to a large extent stabilized the palladium centers against agglomeration under ethylene hydrogenation conditions.

As stated earlier, the catalytic properties of COFs rely on the chemical and physical nature of the constituent building blocks, which are judiciously selected to optimize catalyst activity and stability. Among the most common building units are arylamines and arylaldehydes used in imine- and β-ketoenamine-linked COFs; these monomers are typically synthesized using coupling reactions (*i.e.* C–C, C–N, *etc.*) or under reducing conditions involving supported palladium, like palladium on carbon (conversion of a nitro group to an amine group). For example, one of the extensively used amine building units is 1,3,6,8-tetrakis(4-aminophenyl)pyrene (PyTTA), which is used to synthesize Py-1P COF. During the synthesis of the PyTTA monomer, a homogeneous palladium catalyst ($Pd(Ph_3)_4$) is used in the Suzuki cross-coupling reaction involving 1,3,6,8-tetrabromopyrene and 4-aminophenylboronic acid pinacol ester, raising the possibility of PyTTA contamination with palladium despite extensive purification steps before Py-1P COF synthesis. It is important to note that removing palladium from organic products following Pd-catalyzed reactions, particularly pharmaceuticals,[29] remains a significant challenge and raises toxicity concerns, while residual palladium impurities in organic building blocks used in COFs synthesis would compromise catalyst design and selectivity. Therefore, investigating potential metal contamination levels and their effect on the catalytic performance of both pristine and metal-loaded COFs is crucial and remains unexplored.

In this study, we report the synthesis of a high surface area (Brunauer–Emmett–Teller (BET) of ~2000 $m^2\ g^{-1}$) $PdCl_2$@Py-1P COF with 1 and 4 wt% atomically dispersed Pd. To minimize impurities in the monomer prior to Py-1P COF synthesis, we implemented strategies based on PPh_3 treatment and acid purification to reduce residual Pd contaminants. The 1 and 4 wt% loadings were chosen to minimize the risk of single atom agglomerations and observe single atom performance at low weight loadings. The $PdCl_2$@Py-1P COF catalyst was characterized using various spectroscopic techniques, including X-ray photoelectron spectroscopy (XPS), powder-X-ray diffraction (PXRD) and Fourier transform infrared spectroscopy (FTIR) of adsorbed CO, and its catalytic performance was evaluated for ethylene hydrogenation. Acid purification was effective in removing 90% of the Pd impurities, thereby minimizing the catalytic activity of the pristine Py-1P COF and enabling the measurements of the intrinsic activity of the isolated Pd complexes. This work highlights the critical role of purification and its underlying mechanisms in shaping the coordination environment and structural integrity of COFs, which in turn significantly impacts their catalytic activity and selectivity in ethylene and acetylene hydrogenation.

Experimental

Materials and methods

Chemicals. All starting materials were used without further purification unless otherwise specified. 1,3,6,8-Tetrabromopyrene (95%), 4-aminophenylboronic acid pinacol ester (98%), and tetrakis(triphenylphosphine)palladium(0) (98%) were purchased from AmBeed. Potassium carbonate (99%), terephthalaldehyde (98%), and triphenylphosphine (99+%) were purchased from Alfa Aesar. 1,2-Dichlorobenze (99%), bis(benzonitrile)palladium(II) dichloride (99+%), and Celite® 545 were purchased from Acros Chemicals. 1,4-Dioxane (99+%) was purchased from Thermo Scientific. Toluene (Certified ACS, 99.9%) and hydrochloric acid (Certified ACS Plus, 36.5–38.0% w/w) were purchased from Fisher Scientific. Finally, *n*-butanol (99.9%) and anhydrous chloroform (≥99%) were purchased from Sigma Aldrich. The PYREX tubes used were of inner diameter 9.7 mm, outer diameter 12 mm, and length 26.5 cm. 1,3,6,8-Tetrakis(4-aminophenyl)pyrene[30] and Py-1P COF were prepared according to modified literature methods.[31,32]

Synthesis and purification of 1,3,6,8-tetrakis(4-aminophenyl) pyrene (PyTTA)

PyTTA synthesis. To synthesize Py-1P COF, the 1,3,6,8-tetrakis(4-aminophenyl)pyrene (PyTTA) monomer must first be synthesized *via* a Suzuki–Miyaura cross-coupling reaction (Fig. 1). This is done by placing 1,3,6,8-tetrabromopyrene (1.0 g, 1.93 mmol), 4-aminophenylboronic acid pinacol ester (2.0 g, 9.13 mmol), and potassium carbonate (1.44 g, 10.4 mmol) in a solution of 1,4-dioxane and water (80 mL : 16 mL). The system was purged by bubbling N_2 gas for a minimum of 30 minutes while the catalyst system was prepared. In an argon-filled glovebox, tetrakis(triphenylphosphine)palladium(0) (0.2 g, 0.18 mmol) was placed in 1,4-dioxane (10 mL) and stirred for 10 minutes. The catalyst solution was then cannulated to the reaction system, which was then fitted with a condenser

Open Access Article. Published on 16 December 2025. Downloaded on 2/14/2026 6:47:07 PM.
This article is licensed under a Creative Commons Attribution-NonCommercial 3.0 Unported Licence.

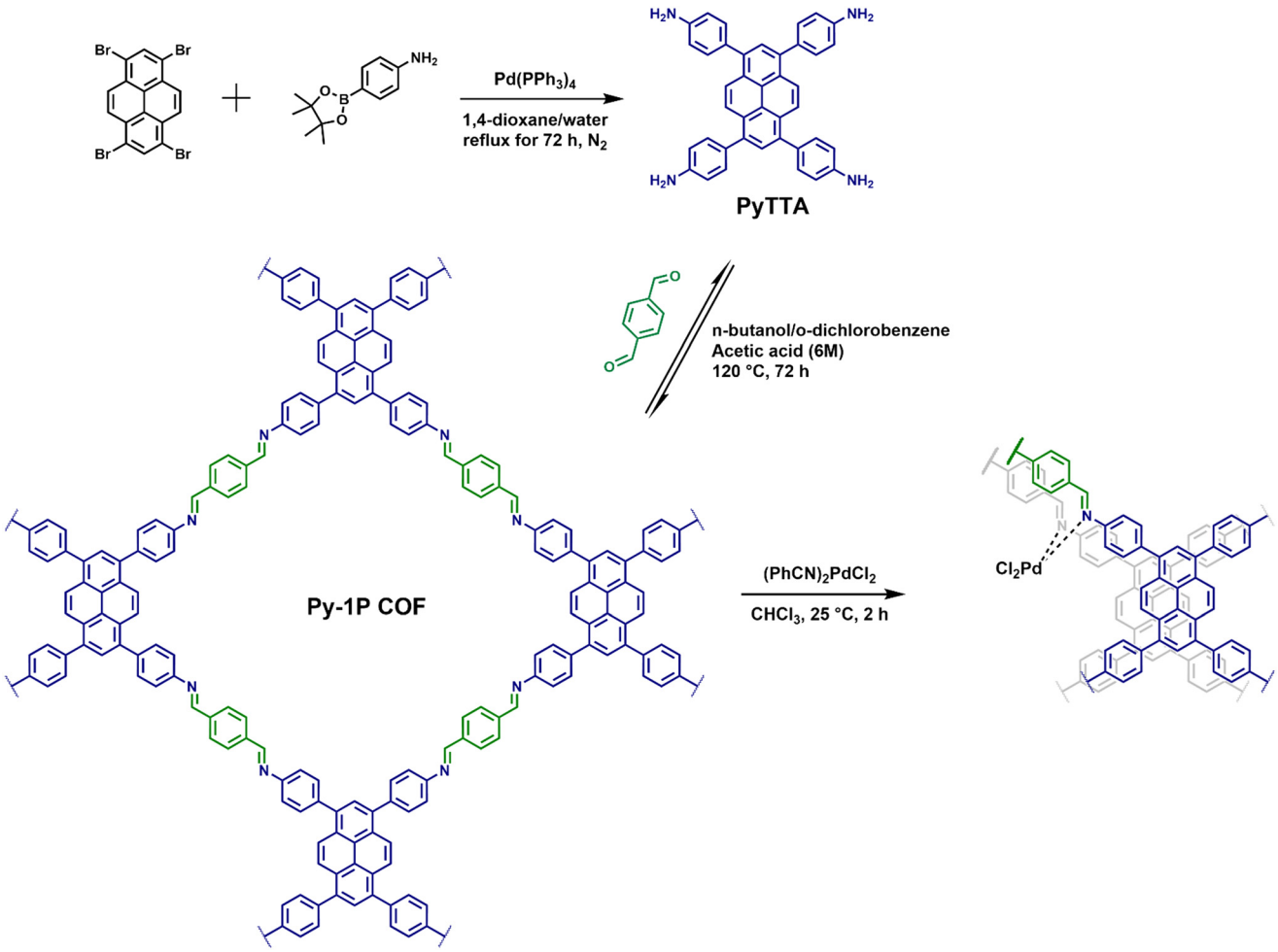

Fig. 1 $PdCl_2$@Py-1P COF synthesis. Synthesis of the PyTTA monomer, Py-1P COF, and $PdCl_2$@Py-1P COF.

and allowed to react under continuous N_2 flow @ 105 °C for 72 h. Afterwards, the solution was cooled to room temperature and filtered through Celite. Water was then added to the filtrate to precipitate the monomer and the solution was filtered again, collecting the solid at this time. The monomer was then dried under vacuum at 80 °C (1.0 g, 91% yield). It is noted that this synthesis introduces a palladium contamination of 0.46 wt% based on ICP-OES from the homogeneous catalyst, tetrakis(triphenylphosphine) palladium(0), used in the reaction, which requires purification.

Acid purification of PyTTA. To find a method to remove the palladium contamination, the synthesized monomer (500 mg) was placed in a beaker with 125 mL of deionized water. Hydrochloric acid (2 M) was added dropwise into the water in a minimal amount until the monomer dissolved. The monomer was sonicated, as needed, to disperse larger chunks while dissolving. The solution was then placed into a column (16.5 cm L, 28.1 mm D) filled with 5 inches of Celite and allowed to pass through. After collecting the filtrate, the monomer was precipitated with 0.25 M sodium hydroxide until the pH tested to 14 *via* indicator paper (~50 mL). The monomer was then filtered through a medium porosity glass frit and freeze dried (447.1 mg, 89% yield). This method reduced the palladium contamination to 0.05 wt% based on ICP-OES.

Triphenylphosphine purification of PyTTA. The PyTTA monomer (613.1 mg) was suspended in 100 mL toluene in a Schlenk flask while being purged with nitrogen for 30 minutes. Triphenylphosphine (601.4 mg) was added to the flask. The system was then flushed with nitrogen before being sealed and allowed to stir at room temperature for 12 h. The solution was then filtered and the monomer dried under vacuum at 80 °C (472.0 mg, 77% yield). This method reduced the palladium contamination to 0.36 wt% by ICP-OES.

Synthesis of Py-1P COF

Py-1P COF was synthesized according to published methods with some modification (Fig. 1). The Py-1P COF was synthesized *via* a solvothermal PYREX tube method. Each PYREX tube was charged with 45.2 mg of the dried, synthesized PyTTA monomer and 21.5 mg

 This journal is © The Royal Society of Chemistry 2026

Open Access Article. Published on 16 December 2025. Downloaded on 2/14/2026 6:47:07 PM. This article is licensed under a Creative Commons Attribution-NonCommercial 3.0 Unported Licence.

terephthalaldehyde. Then 2 mL *n*-butanol and 2 mL *o*-dichlorobenzene were added and sonicated for 10 minutes to create uniform suspension. After the suspension was achieved, 0.4 mL acetic acid (6 M) was added and the tube flash frozen in liquid nitrogen. This was the beginning of the first of three freeze–pump–thaw cycles to degas the system. Following the third cycle, the tube was flame-sealed and placed in an oven at 120 °C for 72 h. Upon completion of the reaction, the tubes were left to cool down to room temperature, broken, filtered, washed with acetone until the filtrate ran clear, and placed in a Soxhlet extractor with THF for 24 h. The product was then dried under vacuum at 80 °C for 12 h to yield Py-1P COF as a golden powder (47.2 mg, 90% yield). ICP-OES was then performed to determine Pd content.

Synthesis of $PdCl_2$@Py-1P COF

The preparation of $PdCl_2$@Py-1P COF is shown in Fig. 1 and was performed in an inert argon-filled glovebox. This loading procedure was adapted from the method previously reported by this group.[28] For the 1 wt% Pd loading, anhydrous chloroform (20 mL) was used to suspend 150 mg of the COF in a Schlenk flask. A solution of bis(benzonitrile)palladium(II) chloride (5.5 mg, 0.014 mmol) in anhydrous chloroform (18 mL) was made according to the targeted weight loading. The palladium solution was then added to the Py-1P COF suspension dropwise to optimize even dispersion of the single atoms. The solution was then filtered over a medium glass frit then washed in a chloroform Soxhlet extractor for 12 hours. The sample was dried under vacuum (10^{-2} mbar, 80 °C). ICP-OES was then performed to determine Pd content. This same procedure was followed for the 4 wt% Pd loadings with 22 mg (0.057 mmol) bis(benzonitrile)palladium(II)chloride being dissolved in 72 mL of anhydrous chloroform. It is noted that the previous work performs the chloroform Soxhlet in a nitrogen environment that was not replicated in this work.

Characterization methods

Surface area analyses and pore size distributions were collected on a Micromeritics 3Flex with a Smart VacPrep degassing chamber. All samples were degassed at 90 °C for 300 minutes and 120 °C for 600 minutes before undergoing analysis. Powder X-ray diffraction spectra were collected on a Panalytical X'pert pro multipurpose diffractometer (Cu Kα radiation). Samples were mounted on a zero-background sample holder and measured with a 2θ range of 0–70. A Thermo Scientific ESCALAB 250 microprobe was used to collect the XPS spectra. ICP-OES data was collected on an Agilent Technologies 5110 ICP-OES equipped with an SPS 4 autosampler. The samples were digested in 10 mL *aqua regia* at 60 °C for 12 h before being diluted to 100 mL and filtered through filter paper.

DRIFTS of CO adsorption was conducted using a Thermo Fisher Scientific Nicolet iS50 FTIR spectrometer equipped with a liquid nitrogen-cooled mercury–cadmium–telluride (MCT) infrared detector. The catalyst was loaded into the sample cup of an *in situ* Praying Mantis diffuse reflection cell (Harrick Scientific Products). Prior to CO chemisorption, the catalyst was dried under a 100 sccm N_2 flow at 120 °C for 2 h. Following the N_2 treatment, the sample was cooled to −120 °C using liquid nitrogen under a continuous N_2 flow. A background spectrum was collected at −120 °C under N_2 and subtracted from all subsequent spectra. The catalyst was then exposed to 1 kPa CO (balanced in N_2) for 10 min, followed by N_2 purging to remove gas-phase CO. A series of CO adsorption spectra were recorded continuously, with each spectrum averaged over 32 scans at a data spacing of 0.482 cm^{-1}.

The catalytic performance of the $PdCl_2$@Py_COF catalyst and their respective Pristine COF was evaluated for ethylene hydrogenation in a quartz packed-bed reactor under differential conditions:

$$C_2H_4 + H_2 \rightarrow C_2H_6\ (\Delta H^\circ = -137\ \text{kJ mol}^{-1})$$

To minimize transport limitations, the 4.0 wt% and 1.0 wt% $PdCl_2$@Py-1P COF catalyst was diluted intra-pellet with silica gel (SiO_2, 0.075–0.250 mm, 150 Å, ACROS Organics), which was calcined in air at 800 °C prior to use. The catalyst–SiO_2 mixture was prepared to achieve a final Pd loading of 0.08 wt% and 0.5 wt% respectively. The materials were ground using an agate mortar and pestle, pelletized, and sieved to obtain 180–300 μm pellets. A total of 0.075 g of the diluted catalyst mixture was loaded into a 0.75 inch OD glass packed-bed reactor. Before catalytic testing, the catalyst was dried at 120 °C under a 100 sccm He flow for 2 h and subsequently cooled to 22 °C under He flow.

All catalytic activity measurements were conducted at atmospheric pressure. The gas composition of the reactor effluent was analyzed using an online gas chromatograph (MicroGC Fusion Gas Analyzer, Inficon). Ethylene (C_2H_4) and ethane (C_2H_6) were separated using an Rt-alumina Na_2SO_4 packed column and quantified with a thermal conductivity detector (TCD). High-purity feed gases—H_2 (UHP, 99.999%), 20% C_2H_4 (certified gas, Airgas), and He (UHP, 99.999%)—were obtained from Airgas. H_2 and He were further purified using high-capacity moisture and oxygen traps (Restek catalog #20600). All gas flows were regulated by mass flow controllers (5850EM, Brooks Instrument).

Ethylene conversion and reaction rate were assessed based on the rate of reaction per gram of COF per second to distinctly compare the catalytic activity of the pristine COF and the Pd-loaded sample. This normalization to the total COF mass enables a direct evaluation of catalytic performance, providing insight into the contribution of Pd impurities in the pristine COF to its inherent activity.

$$\text{Conversion} = \frac{\text{mole of } C_2H_6 \text{ (outlet)}}{\text{mole of } C_2H_4 \text{ (inlet)}}$$

$$\text{Reaction Rate} = \frac{C_2H_6 \text{ formation rate (mol } C_2H_6\ s^{-1})}{\text{weight of COF (Before dilution)(mg)}}$$

The hydrogenation reaction was performed at 22 °C with a

Open Access Article. Published on 16 December 2025. Downloaded on 2/14/2026 6:47:07 PM.
This article is licensed under a Creative Commons Attribution-NonCommercial 3.0 Unported Licence.

Table 1 Pd content and purification efficiency for Py-1P COFs under different monomer purification methods

Purification method	Purified monomer Pd content (wt%)	Initial monomer Pd content (wt%)	Percent removal	COF sample	COF Pd content (wt%)
Acid	0.05 ± 0.04	0.46 ± 0.02	89	Pristine COF	0.04 ± 0.04
				Pd loaded	4.92
PPh_3	0.36 ± 0.08	0.46 ± 0.02	22	Pristine COF	0.23 + 0.04
				Pd loaded	3.40
Unpurified	N/A	0.46 ± 0.02	N/A	Pristine COF	0.35
				Pd loaded	4.19

partial pressure of C_2H_4 at 5 kPa and H_2 at 5 kPa. Ethane was the sole detected product, and no measurable conversion of C_2H_4 or H_2 was observed in the absence of the catalyst, *i.e.* empty reactor tube or quartz wool-packed reactor.

Results and discussion

The effect of monomer purification on the final palladium (Pd) content and structural integrity of the synthesized Py-1P COFs was systematically investigated. Table 1 summarizes the Pd content of pristine and Pd-loaded COFs, as well as the Pd levels in purified and unpurified monomers (PyTTA) and the associated percent removal. Among the purification methods tested, acid purification was the most effective, reducing the Pd content in the monomer from 0.46 wt% to 0.05 wt%, corresponding to an 89% removal efficiency. In contrast, PPh_3 purification achieved only a 22% removal. The acid purification method is believed to remove palladium impurities by dissolving the monomer, while the insoluble palladium species are retained on the Celite stationary phase during column filtration. This would be similar to how the Pd is removed by reactions using Pd catalysts.[33–37] In contrast, the PPh_3 purification method in an attempt to improve the solubility of Pd contaminants by facilitating coordination between PPh_3 and Pd species present on the suspended PyTTA monomer. However, this approach may be less effective at removing palladium if the resulting $Pd(PPh_3)$ complexes are not efficiently separated from the monomer during the filtration process.

Physical properties of Py-1P COF & 4 wt% $PdCl_2$@Py-1P COF

Analysis was performed before and after the samples were loaded with palladium, and a post-loading decrease in surface area was consistently observed across all samples (Fig. 2 and S1). All nitrogen adsorption–desorption isotherms were

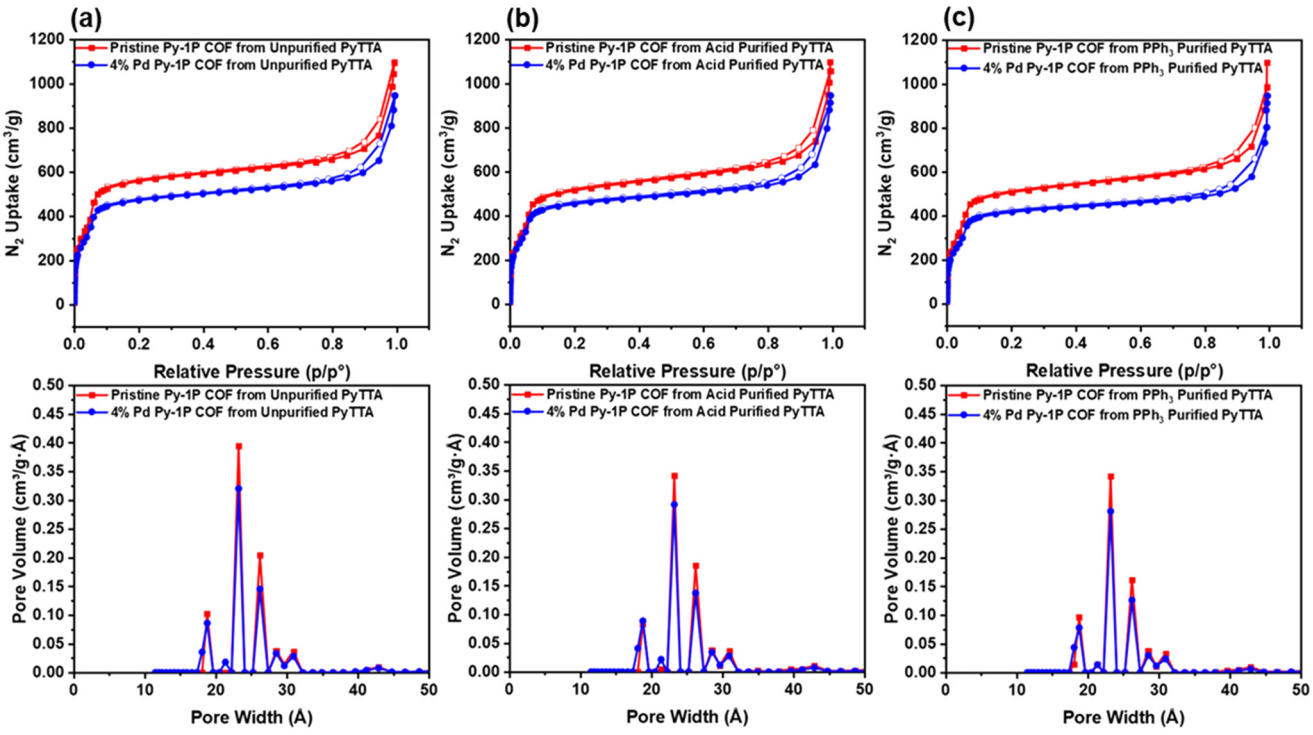

Fig. 2 N_2 absorption isotherms and pore size distributions of the pristine (red) and 4% Pd (blue) Py-1P COF from (a) unpurified, (b) PPh_3 purified, and (c) acid purified PyTTA.

 This journal is © The Royal Society of Chemistry 2026

Open Access Article. Published on 16 December 2025. Downloaded on 2/14/2026 6:47:07 PM.
This article is licensed under a Creative Commons Attribution-NonCommercial 3.0 Unported Licence.

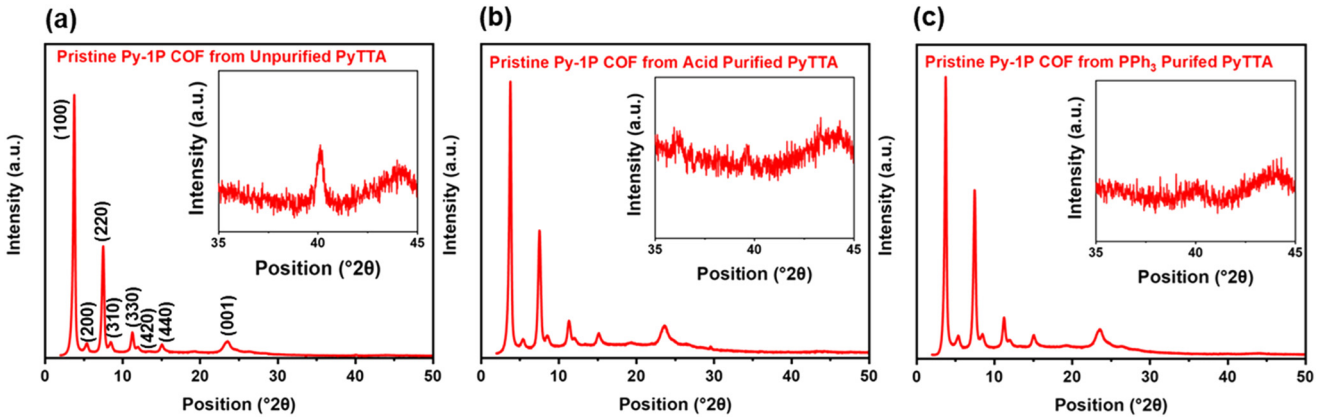

Fig. 3 Powder X-ray diffraction spectra of the pristine Py-1P COFs from (a) unpurified, (b) acid purified, and (c) PPh_3 purified PyTTA. Each spectrum has an inset of the zoomed-in region of the peak at $2\theta = 40°$.

classified as type IVb.[38] However, the extent of the surface area reduction varied depending on the purification method used. For the unpurified COF sample, the pristine surface area (Fig. 2a) was 2294 ± 228 $m^2\ g^{-1}$, which decreased to 1813 $m^2\ g^{-1}$ after palladium loading—a 21% reduction. This effect was less pronounced in samples where the PyTTA monomer was purified prior to COF synthesis. With PPh_3 purification, the surface area dropped by 12%, from 1887 ± 203 $m^2\ g^{-1}$ to 1666 $m^2\ g^{-1}$ (Fig. 2b). The acid purification method resulted in the smallest decrease—only 6%—from 1936 ± 133 $m^2\ g^{-1}$ to 1812 $m^2\ g^{-1}$ (Fig. 2c). These results suggest that monomer purification is an important factor for preserving surface area in the final COF material. The slight surface area reduction in the pristine COFs from purified monomers may be due to amines undergoing slight oxidation during purification upon exposure to air and light. The partial oxidation of amine sites introduces terminal groups that impede framework extension and lower the surface area of the COF. Pore size distribution was calculated using nonlocal density functional theory (NLDFT; N_2@77 K—carbon cylinder pores, single wall nanotube model) and was found to be consistent across both pristine and Pd-loaded samples. All samples exhibited a pore width of approximately 2.3 nm, confirming the mesoporous nature of the COFs. Surface area and pore size distribution were only collected before and after $PdCl_2$ loading and not after catalytic reactivity experiments.

Powder XRD was used to characterize the crystallinity of the COF samples. All samples have the characteristic peaks of Py-1P COF for the (110), (200), (220), (310), (330), (420), (440), and (001) (Fig. 3 and S2).[39] The (001) plane is where the *z*-stacking of COF sheets is observed and is where the Pd SACs are coordinating to two nitrogen atoms between COF layers. Due to the contamination from the palladium catalysts in the PyTTA monomer synthesis, there is a peak at $2\theta = 40°$ that is attributed to the (111) of palladium(0) nanoparticles (inset in Fig. 3).[40–42] This peak was monitored across purification methods in the pristine samples. As expected, the sample that has the most intense agglomeration peak is the unpurified PyTTA pristine COF. The acid purified PyTTA pristine COF had this peak disappear completely due to its low Pd contamination content. The COF sample from PPh_3 purified PyTTA has an intensity at this position that is lower and broader than that of the sample from unpurified PyTTA indicating that the remaining Pd particles are smaller in size than in the original COF. These XRD findings support the ICP-OES analysis of the Pd content in each sample and each purification method's effectiveness. These findings further highlight the importance of monomer purification before COF synthesis, as residual palladium impurities can significantly influence the catalytic activity of the resulting COFs. PXRD was only collected before and after $PdCl_2$ loading and not after catalytic reactivity experiments.

Local coordination and local properties of Pd

Fig. 4 shows the Pd_{3d} XPS spectra of the unpurified PyTTA monomer. The unpurified monomer spectrum displays low-intensity peaks at binding energies of 338.1 eV and 343.2 eV, corresponding to the respective Pd $3d_{5/2}$ and Pd $3d_{3/2}$ orbitals. These peaks are not observed in the spectra of either of the purified monomers (Fig. S4a and b). These binding energies indicate that the Pd is present in a coordinated form

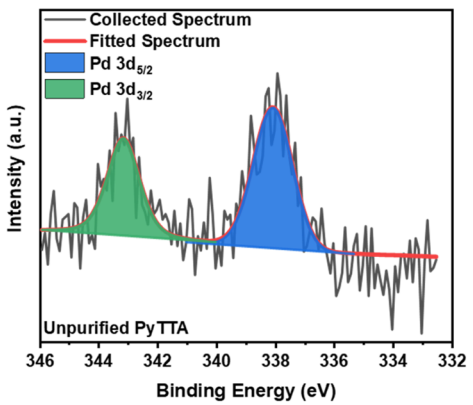

Fig. 4 Pd_{3d} XPS spectrum for unpurified PyTTA.

Open Access Article. Published on 16 December 2025. Downloaded on 2/14/2026 6:47:07 PM.
This article is licensed under a Creative Commons Attribution-NonCommercial 3.0 Unported Licence.

to N rather than as PdO or metallic Pd.[43] This confirms that palladium is introduced during monomer synthesis and exists in a chemically bound state. It can be inferred that this is most likely the state of Pd entering COF synthesis, where it then unbinds from the N, moves throughout the solution, and agglomerates upon PyTTA dissolution to create the nanoparticle (111) reflections seen in the PXRD spectra in Fig. 3. After acid and triphenylphosphine purification, no distinct peaks within the Pd region were observed in the PyTTA monomers. Similarly, the pristine COF spectra showed no distinct peaks within the Pd region across all monomer purification methods (Fig. S4d–f), making it difficult to assess the effect of purification on the state of remaining Pd impurity in the monomers or COF samples.

Fig. 5 shows the Pd 3d XPS spectra of 4% Pd-loaded Py-1P COF under three different purification conditions: unpurified, PPh_3 purified, and acid purified. Each spectrum features two distinct Pd spin–orbit doublets, corresponding to palladium in different chemical environments consistent with PdO and PdN.[43–45] The PdO peaks are believed to have been introduced from the ambient environment of the post-loading Soxhlet extraction step used for purification. The PdO signals appear at lower binding energies, with Pd $3d_{5/2}$ and Pd $3d_{3/2}$ peaks around 336.5–337.1 eV and 341.8–342.1 eV, respectively. In contrast, the PdN signals are shifted to higher binding energies, near 338.2–338.4 eV and 343.4–343.5 eV. These ranges are comparable to those reported for PdO (336.4–336.5 and 341.8 eV) and PdN (337.8 and 343.1–343.3 eV).[43] In both the unpurified and acid purified samples, the PdN peaks are more intense, suggesting a greater extent of palladium coordination with nitrogen within the COF framework. Conversely, the PPh_3 purified sample exhibits a diminished PdN signal, indicating a lower degree of Pd–N interaction. These results demonstrate that the purification method significantly influences the local chemical environment of palladium, which may in turn affect the catalyst's performance. This purification method may reduce the Pd–N interaction within the COF by creating some Pd sites where residual PPh_3 is bound in various states. However, when scans were collected in the phosphorous region, no signal was detected, suggesting this would be in an instance below the limit of detection.

The high-resolution N_{1s} XPS spectra for the pristine Py-1P COF samples (Fig. 6a) show a consistent peak at approximately 399.2 eV across all purification conditions—acid purified, PPh_3 purified, and unpurified—indicating that the nitrogen environment in the imine linkage remains structurally similar regardless of the monomer purification method. This peak corresponds to the nitrogen in the C=N imine bond, which is the dominant nitrogen species in the COF framework.[28] The palladium-loaded samples (Fig. 6b) exhibit a single nitrogen peak that appears broadened due to the presence of two distinct binding environments: one corresponding to uncoordinated imine nitrogen (~399 eV) and the other to imine nitrogen coordinated to palladium (~400 eV).[28] This shift confirms the successful coordination of Pd(II) species to the nitrogen atoms of the COF. The acid purified sample with 1 wt% Pd loading (Fig. 6c) showed a less intense Pd-coordinated N1s peak compared to the 4 wt% sample which is consistent with the difference in Pd loading. Among the Pd-loaded samples, the PPh_3-purified COF shows a noticeably broader N_{1s} peak compared to the acid-purified and unpurified samples. This broadening may be attributed to a more heterogeneous nitrogen environment, possibly arising from defect sites or varying local bonding environments introduced during the purification process. These subtle spectral differences offer further insight into how monomer purification impacts the structural uniformity of the resulting COFs and their capacity to host atomically dispersed metal sites.

To assess the impact of different purification methods and metal loading on the morphology of Py-1P COF and the distribution of palladium, we employed scanning electron microscopy (SEM, Fig. S5) and energy-dispersive X-ray (EDX) elemental mapping (Fig. S6–S10). SEM images revealed irregular sheet-like particles with some surface aggregation in palladium-loaded samples. Despite differences in morphology, all materials exhibited high internal pore accessibility, as confirmed by the consistently high BET surface area values (Fig. 2 and S1). EDX mapping was further

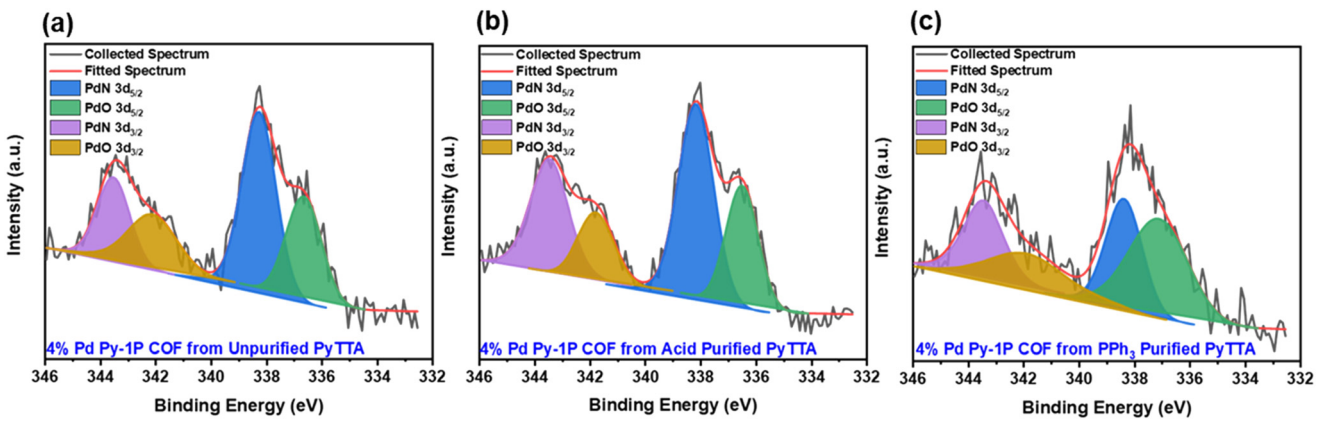

Fig. 5 Pd_{3d} XPS spectra for 4 wt% Pd Py-1P COF from (a) unpurified (b) acid purified (c) PPh_3 purified PyTTA.

 This journal is © The Royal Society of Chemistry 2026

Open Access Article. Published on 16 December 2025. Downloaded on 2/14/2026 6:47:07 PM.
This article is licensed under a Creative Commons Attribution-NonCommercial 3.0 Unported Licence.

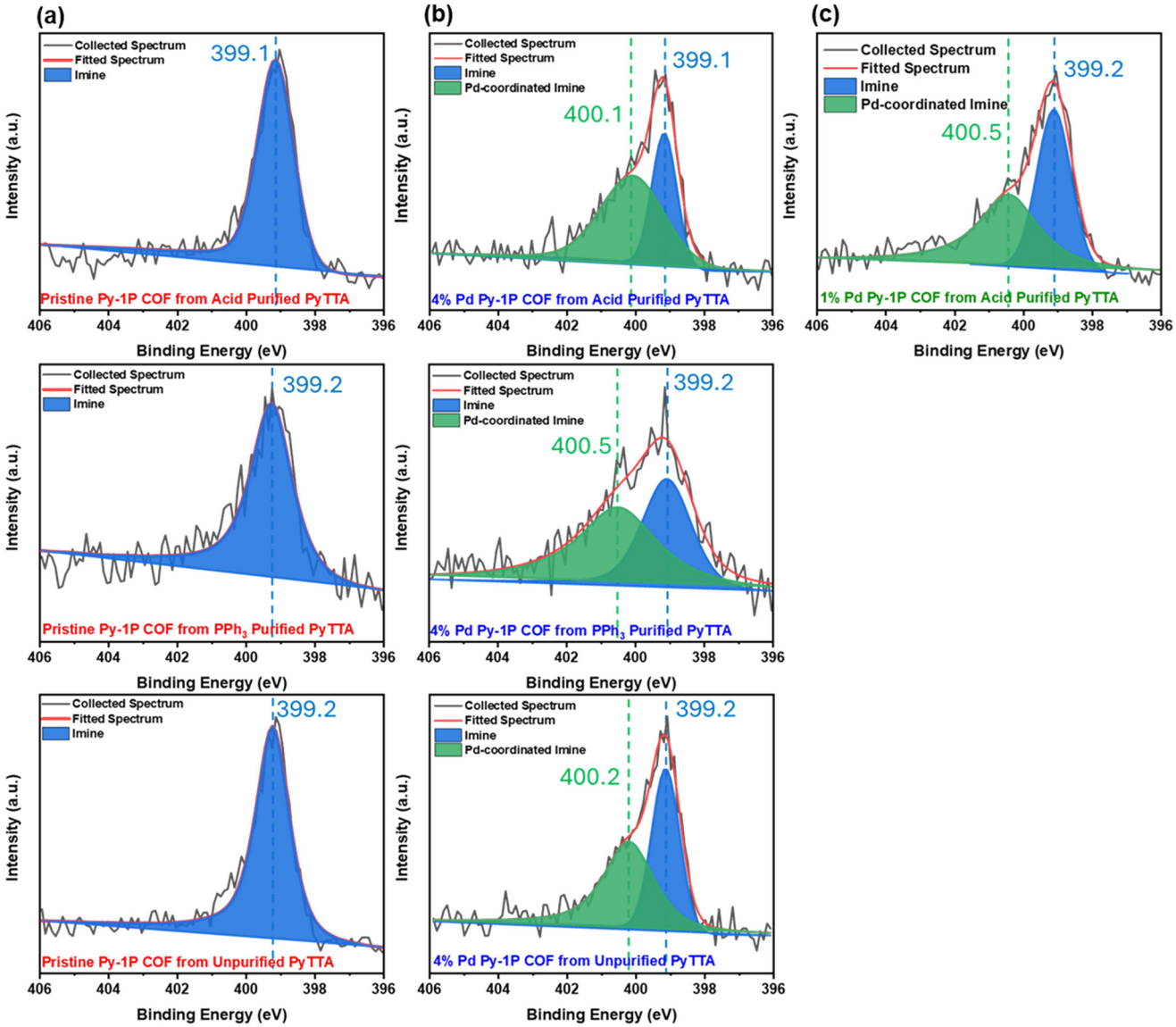

Fig. 6 N_{1s} XPS spectra for (a) pristine, (b) 4 wt% Pd, and (c) 1 wt% Pd Py-1P COF from variously purified PyTTA, acid purified (top), PPh_3 purified (middle) and unpurified (bottom).

used to examine the spatial distribution of palladium and potential agglomeration in both pristine Py-1P COF and Pd-loaded samples, particularly those with higher metal loading (*e.g.*, 4 wt%). The EDX results confirmed the presence of residual Pd in all pristine Py-1P COF samples, irrespective of the purification method, consistent with ICP measurements which revealed Pd contents in the range of 0.04–0.35 wt% (Table 1). For both 1 and 4 wt% Pd-loaded samples, EDX images (Fig. S9 and S10) demonstrated a uniform Pd distribution without noticeable agglomeration, underscoring the ability of the Py-1P COF to stabilize well-dispersed single Pd sites for subsequent application in ethylene hydrogenation studies.

To evaluate the homogeneity of the local coordination environment of Pd atoms in the $PdCl_2$@Py-1P COF catalyst, CO adsorption experiments were conducted at −120 °C using diffuse-reflectance infrared Fourier transform spectroscopy (DRIFTS). A symmetric and relatively narrow absorption band was observed at 2129 cm^{-1}, with a full width at half maximum (FWHM) of approximately 20 cm^{-1}, as shown in Fig. 7. A minor shoulder observed at higher wavenumbers is attributed to the presence of small oxidized Pd species, likely introduced during the chloroform Soxhlet extraction step after $PdCl_2$ loading conducted under ambient conditions. These oxidized Pd species would maintain the +2 oxidation state of the Pd but change the local electronic properties on the Pd, causing the noticeable shoulder peak at slightly higher wavenumbers. This is because O is more electronegative than Cl and, therefore, pulls more electron density away from the Pd atom. No additional CO adsorption bands were detected in the 1800–2200 cm^{-1} region, where vibrational features associated with linear, bridge, and hollow

Open Access Article. Published on 16 December 2025. Downloaded on 2/14/2026 6:47:07 PM.
This article is licensed under a Creative Commons Attribution-NonCommercial 3.0 Unported Licence.

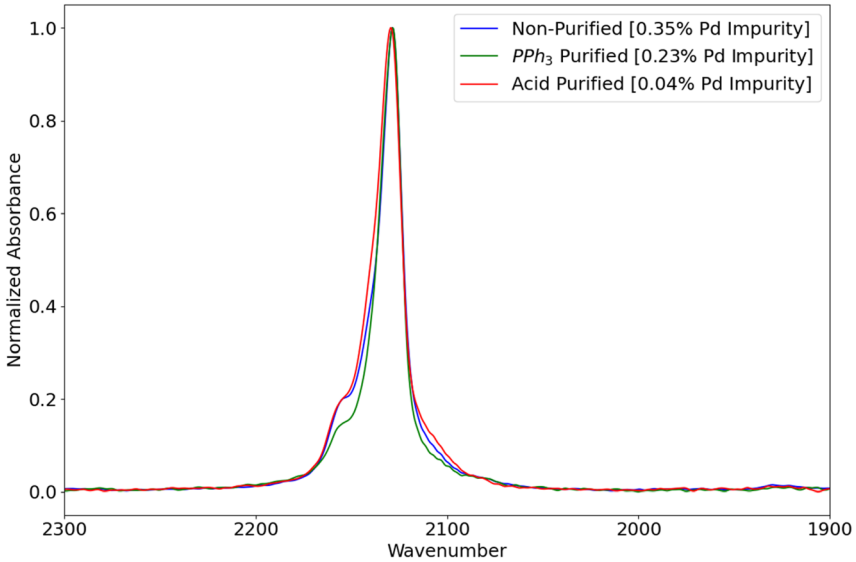

Fig. 7 DRIFTS spectra of CO adsorption on the 4% $PdCl_2$@Py-1P COF catalyst for different purification process of PyTTA.

site adsorption on Pd typically appear.[46–50] This absence indicates that Pd is predominantly present as isolated single atoms. "Noteworthy, because the native Pd impurities exist only at trace levels and are not uniformly distributed, their contribution to the DRIFTS signal is negligible; after $PdCl_2$ metalation, the greatly increased population of surface-accessible, atomically dispersed Pd sites overwhelmingly dominates the CO-DRIFTS response, effectively masking any signal from the minor Pd-cluster impurities". Furthermore, the consistent peak position and bandwidth across samples prepared using different monomer purification protocols suggest that these treatments have minimal impact on the post-synthetic modification strategy employed to achieve 4 wt% Pd single-atom loading. This is in contrast to the variations seen in the XPS spectra and suggests that the small differences seen in Pd_{3d} and N_{1S} XPS peaks are not large enough to be measured by CO adsorption on the Pd.

Catalytic activity and kinetics of ethylene hydrogenation

Ethylene hydrogenation is a crucial catalytic reaction that can be conducted under mild conditions and is widely employed as a probe reaction for extended metal surfaces and supported metal catalysts, including Pt, Ir, Rh, and Au.[51–60] In this study, the catalytic performance of the 4 wt% $PdCl_2$@Py-1P COF catalyst and its respective pristine COF support was evaluated for ethylene hydrogenation at atmospheric pressure and a constant temperature of 22 °C. Notably, in both the non-purified (0.35 wt% Pd impurity) and PPh_3-purified (0.23 wt% Pd impurity) samples, the activities of the Pd-loaded catalysts were statistically indistinguishable from those of their corresponding pristine COF supports. This trend was further validated through repeated measurements of the 4% Pd-loaded samples, which exhibited minimal experimental variation, with error percentages of 2.6% for the non-purified sample and 2.1% for the PPh_3-purified sample. These low deviations suggest that, in the absence of significant removal of Pd impurities, most of the observed activity originates from the pristine COF, making it challenging to distinguish the catalytic contribution of inherent Pd impurities from that of the intentionally introduced Pd catalyst. However, despite the lower Pd impurity content in the PPh_3-purified COF compared to the non-purified COF, the former exhibited higher catalytic activity. XRD results revealed a much broader peak at 2θ = 40° that is attributed to smaller palladium clusters for the PPh_3 purified pristine COF compared to the unpurified pristine COF. This suggests that PPh_3 purification may reduce the size of Pd impurity clusters, thereby enhancing their catalytic performance, which further masks the catalytic properties of the loaded Pd atoms.

At high (4 wt%) Pd loadings, there is a potential for single atoms to aggregate under reaction conditions. To investigate the catalyst structure under such conditions, DRIFTS of CO adsorption was performed following *in situ* ethylene hydrogenation (5 kPa C_2H_4 and 5 kPa H_2 in N_2 balance at 22 °C), as illustrated in Fig. 8(b). A CO band observed at 1920 cm^{-1} (highlighted by the shaded region) in the higher loading sample is attributed to bridge-bound CO on Pd clusters, suggesting that Pd single atoms undergo aggregation during the reaction. In contrast, the CO adsorption spectrum at the lower Pd loading of 1% indicates the presence of only atomically dispersed Pd sites under identical reaction conditions. This observation underscores the critical role of monomer purification prior to COF synthesis and metal incorporation in stabilizing isolated Pd atoms. Importantly, even at a reduced Pd loading of 1 wt%, the acid-purified sample demonstrated significantly higher (~2.5×) catalytic activity compared to the pristine COF, further validating the effectiveness of the purification strategy.

 This journal is © The Royal Society of Chemistry 2026

Open Access Article. Published on 16 December 2025. Downloaded on 2/14/2026 6:47:07 PM.
This article is licensed under a Creative Commons Attribution-NonCommercial 3.0 Unported Licence.

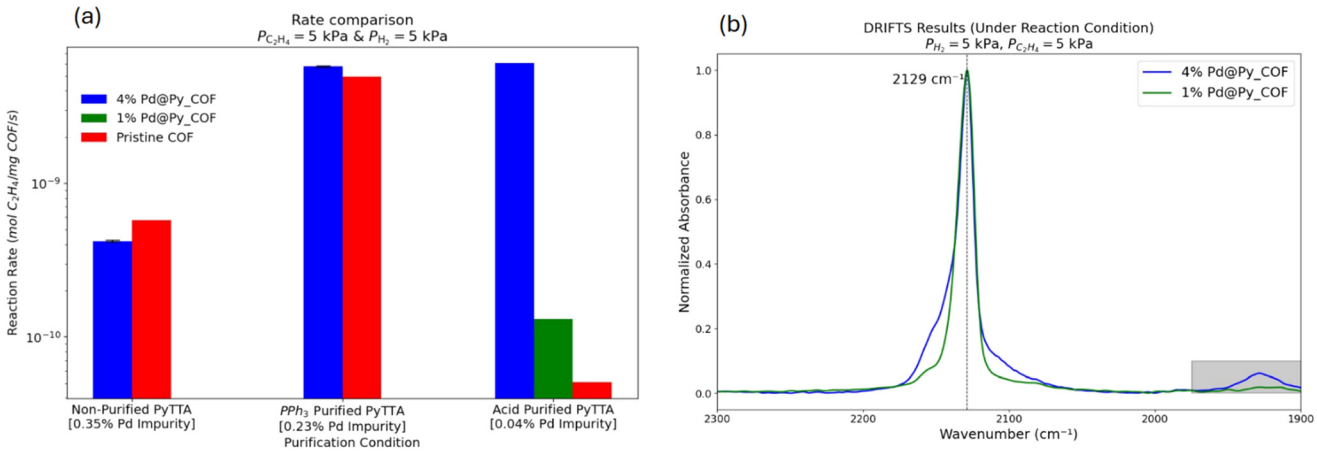

Fig. 8 (a) Comparison of reaction rate for different purification processes for 4% $PdCl_2$@Py-1P COF and their respective pristine COF. (b) Normalized CO-DRIFTS under *in situ* reaction condition (5 kPa C_2H_4 and 5 kPa H_2 in N_2 balance at 22 °C) for 1% $PdCl_2$@Py-1P COF (green) and 4% $PdCl_2$@Py-1P COF (blue) with acid purified PyTTA.

The catalytic hydrogenation of ethylene has been widely investigated, with a well-established reaction pathway involving the stepwise addition of atomic hydrogen across the carbon–carbon double bond.[61–67] Fig. 9 depicts the dependence of turnover frequency (TOF) on the partial pressures of hydrogen and ethylene. Kinetics experiments were performed by varying the C_2H_4 and H_2 partial pressures in the ranges 2.5–5 kPa and 1–5 kPa, respectively. Linear fits to the kinetic data under steady-state conditions reveal a reaction order of approximately 0.57 ± 0.04 with respect to hydrogen and nearly 1.0 ± 0.04 with respect to ethylene. The reaction orders obtained in this study differ from those reported in our previous work on 18 wt% $PdCl_2$@IL-COF, where the reaction orders for hydrogen and ethylene were 0.6 and 0.01, respectively. Notably, the earlier kinetic measurements were performed under lower ethylene partial pressures (0.5–2.5 kPa), whereas the current study demonstrates that the catalyst remains stable under higher ethylene partial pressures (Fig. S11), which may account for the observed differences in kinetic behavior. To further probe the structural evolution of the active sites, DRIFTS experiments were performed on 1 wt% Pd@Py-COF [PPh_3 purified] under reducing environments at 50 °C and 100 °C (Fig. S12(a)). These measurements indicate that isolated Pd sites gradually evolve into small nanoparticles under reductive conditions. Correspondingly, the catalytic activity increased by approximately one order of magnitude after reduction at 50 °C, consistent with the higher intrinsic hydrogenation activity typically associated with Pd nanoparticles (Fig. S12(b)). In addition, the 1% Pd@Py-COF

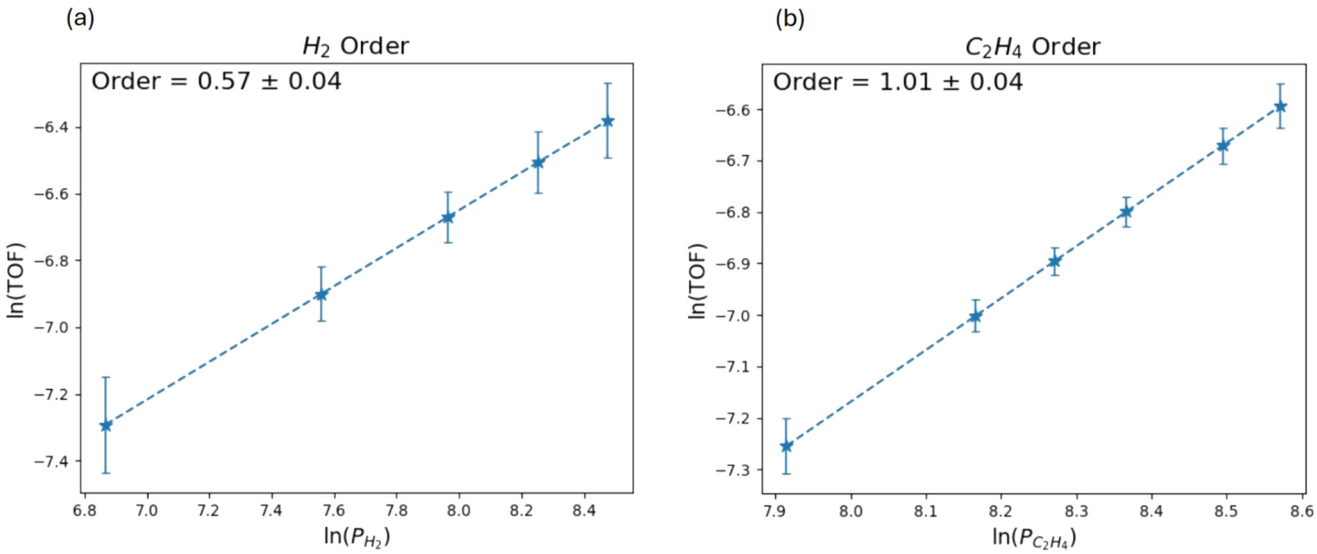

Fig. 9 Kinetic analysis of ethylene hydrogenation over 1 wt% Pd@Py-1P COF catalyst. (a) TOF as a function of hydrogen partial pressure at a fixed ethylene partial pressure of 5 kPa, with a corresponding reaction order of 0.57 in hydrogen. (b) TOF as a function of ethylene partial pressure at a fixed hydrogen partial pressure of 5 kPa, yielding a reaction order of 1.01 with respect to ethylene.

Open Access Article. Published on 16 December 2025. Downloaded on 2/14/2026 6:47:07 PM. This article is licensed under a Creative Commons Attribution-NonCommercial 3.0 Unported Licence.

[acid purified] catalyst exhibited an ~1.3-fold increase in activity after 3 h of continuous operation, suggesting the formation of a limited population of small nanoparticles under reaction condition while the majority of Pd species remain atomically dispersed (Fig. S13). Nanoparticle formation is not evident in the DRIFTS measurements [Fig. 8(b)] because the catalyst was exposed to the reaction environment for only ~1 h during the DRIFTS experiment, whereas the repeat catalytic measurements were collected after ~3 h on stream. The longer exposure time during catalysis enables partial aggregation of Pd sites, which is not captured in the shorter DRIFTS experiment. Such observations highlight that while nanoparticle formation enhances overall hydrogenation rates, single-atom Pd sites are particularly attractive for selective semi-hydrogenation, where control over product distribution is crucial—underscoring the importance of proper COF purification to preserve isolated metal centers.

Supported Ir-based[68,69] and Rh-based[56,57] catalysts, stabilized by two oxygen ligands from the support and two ethylene ligands, have demonstrated activity at 353 K and atmospheric pressure, consistently showing a hydrogen reaction order near 0.5 and a near-zero order for ethylene. These trends suggest that ethylene adsorption is not rate-limiting, while hydrogen undergoes dissociative adsorption on the metal surface.[28] In the present study, the observed positive reaction order with respect to ethylene may indicate comparatively weaker ethylene adsorption on isolated Pd single atoms. The half-order dependence on hydrogen pressure at lower temperatures further implies that hydrogen adsorption is likely equilibrated under these conditions.[70] These findings suggest that at lower Pd loadings, where single atoms are stabilized under reaction conditions and connected with halogen ligands, ethylene hydrogenation may proceed *via* a distinct reaction mechanism compared to that reported on structurally different isolated sites of Ir and Rh. Nevertheless, a more detailed understanding of the active site structure and the role of chloride ligands is essential to fully elucidate the catalytic behavior and is the subject of ongoing work.

Conclusions

Palladium contamination introduced during the synthesis of the PyTTA monomer significantly impacts the performance of Pd single-atom catalysts (SACs) supported on the imine-linked Py-1P COF, underscoring the importance of monomer purification. The purification method chosen not only determines how effectively the contamination is removed but also affects the physical properties of the resulting COF exhibits. Structural changes are observed in BET surface areas, XRD patterns, and XPS spectra. The triphenylphosphine method is demonstrated to be the inferior purification method, not only in effectiveness, but by also having increased negative effects on the properties displayed by the COF supports. This method has a 22% contamination removal, the lowest surface area of the pristine COF, introduces heterogeneity in the Pd environment (as evidenced in XRD and XPS peak broadening), and does not create a significant difference in activity between its pristine and Pd-loaded COFs. In contrast, the acid method has an 89% contamination removal, lesser effect on surface area, preserves homogeneity, and creates a clear distinction in activity levels of the pristine and Pd-loaded COF samples that was so great that it allowed for a second, lower-weight loading sample to be made. This reduced weight loading sample not only displays catalytic stability that the higher loading does not but also maintains a distinct activity level difference from the pristine COF. These results highlight the pivotal role of purification in tuning both the COF framework and the Pd coordination environment, ultimately influencing catalytic performance in ethylene hydrogenation.

Conflicts of interest

There are no conflicts of interest to declare.

Data availability

Supplementary information (SI): SI content includes surface area (Fig. S1), PXRD (Fig. S2), XPS (Fig. S3 and S4), SEM (Fig. S5), EDX (Fig. S6–S10), and DRIFTS (Fig. S11) data. See DOI: https://doi.org/10.1039/d5cy01181g.

Acknowledgements

This research was supported by the National Science Foundation, Division of Chemical, Bioengineering, Environmental, and Transport Division under award numbers CBET-2308630 and CBET-2308631.

References

1 X.-F. Yang, A. Wang, B. Qiao, J. Li, J. Liu and T. Zhang, Single-Atom Catalysts: A New Frontier in Heterogeneous Catalysis, *Acc. Chem. Res.*, 2013, **46**, 1740–1748.
2 B. Choudary, Synthesis and catalytic activity in selective hydrogenation of palladium complexes anchored in montmorillonite, *J. Catal.*, 1991, **130**, 41–51.
3 C. W. A. Chan, A. H. Mahadi, M. M.-J. Li, E. C. Corbos, C. Tang, G. Jones, W. C. H. Kuo, J. Cookson, C. M. Brown, P. T. Bishop and S. C. E. Tsang, Interstitial modification of palladium nanoparticles with boron atoms as a green catalyst for selective hydrogenation, *Nat. Commun.*, 2014, **5**, 5787.
4 A. F. Y. Al-Shammary, I. T. Caga, J. M. Winterbottom, A. Y. Tata and I. R. Harris, Palladium-based diffusion membranes as catalysts in ethylene hydrogenation, *J. Chem. Technol. Biotechnol.*, 1991, **52**, 571–585.
5 J. F. Ciebien, R. E. Cohen and A. Duran, Catalytic properties of palladium nanoclusters synthesized within diblock copolymer films: hydrogenation of ethylene and propylene, *Supramol. Sci.*, 1998, **5**, 31–39.

 This journal is © The Royal Society of Chemistry 2026

Open Access Article. Published on 16 December 2025. Downloaded on 2/14/2026 6:47:07 PM. This article is licensed under a Creative Commons Attribution-NonCommercial 3.0 Unported Licence.

6 Y. Chen, H. Wang, C.-J. Liu, Z. Zeng, H. Zhang, C. Zhou, X. Jia and Y. Yang, Formation of monometallic Au and Pd and bimetallic Au–Pd nanoparticles confined in mesopores via Ar glow-discharge plasma reduction and their catalytic applications in aerobic oxidation of benzyl alcohol, *J. Catal.*, 2012, **289**, 105–117.

7 W. Deng, J. Chen, J. Kang, Q. Zhang and Y. Wang, Carbon nanotube-supported Au–Pd alloy with cooperative effect of metal nanoparticles and organic ketone/quinone groups as a highly efficient catalyst for aerobic oxidation of amines, *Chem. Commun.*, 2016, **52**, 6805–6808.

8 S. Akbayrak, Y. Tonbul and S. Özkar, Nanoceria supported palladium(0) nanoparticles: Superb catalyst in dehydrogenation of formic acid at room temperature, *Appl. Catal., B*, 2017, **206**, 384–392.

9 Q.-Y. Bi, J.-D. Lin, Y.-M. Liu, H.-Y. He, F.-Q. Huang and Y. Cao, Dehydrogenation of Formic Acid at Room Temperature: Boosting Palladium Nanoparticle Efficiency by Coupling with Pyridinic-Nitrogen-Doped Carbon, *Angew. Chem., Int. Ed.*, 2016, **55**, 11849–11853.

10 P. Cotugno, M. Casiello, A. Nacci, P. Mastrorilli, M. M. Dell'Anna and A. Monopoli, Suzuki coupling of iodo and bromoarenes catalyzed by chitosan-supported Pd-nanoparticles in ionic liquids, *J. Organomet. Chem.*, 2014, **752**, 1–5.

11 H. A. Elazab, A. R. Siamaki, S. Moussa, B. F. Gupton and M. S. El-Shall, Highly efficient and magnetically recyclable graphene-supported Pd/Fe3O4 nanoparticle catalysts for Suzuki and Heck cross-coupling reactions, *Appl. Catal., A*, 2015, **491**, 58–69.

12 R. Narayanan and M. Elsayed, Carbon-supported spherical palladium nanoparticles as potential recyclable catalysts for the Suzuki reaction, *J. Catal.*, 2005, **234**, 348–355.

13 Z. Zhang and Z. Wang, Diatomite-Supported Pd Nanoparticles: An Efficient Catalyst for Heck and Suzuki Reactions, *J. Org. Chem.*, 2006, **71**, 7485–7487.

14 L. Zhang, M. Zhou, A. Wang and T. Zhang, Selective Hydrogenation over Supported Metal Catalysts: From Nanoparticles to Single Atoms, *Chem. Rev.*, 2020, **120**, 683–733.

15 G. X. Pei, X. Y. Liu, X. Yang, L. Zhang, A. Wang, L. Li, H. Wang, X. Wang and T. Zhang, Performance of Cu-Alloyed Pd Single-Atom Catalyst for Semihydrogenation of Acetylene under Simulated Front-End Conditions, *ACS Catal.*, 2017, **7**, 1491–1500.

16 H. Yan, H. Cheng, H. Yi, Y. Lin, T. Yao, C. Wang, J. Li, S. Wei and J. Lu, Single-Atom Pd1/Graphene Catalyst Achieved by Atomic Layer Deposition: Remarkable Performance in Selective Hydrogenation of 1,3-Butadiene, *J. Am. Chem. Soc.*, 2015, **137**, 10484–10487.

17 M.-X. Wu and Y.-W. Yang, Applications of covalent organic frameworks (COFs): From gas storage and separation to drug delivery, *Chin. Chem. Lett.*, 2017, **28**, 1135–1143.

18 P. N. Anjana and A. K. Pulikkal, Synthesis, derivation, and applications of imine-linked covalent organic frameworks: A comprehensive review, *Microporous Mesoporous Mater.*, 2025, **387**, 113516.

19 V. Hasija, S. Patial, P. Raizada, A. A. P. Khan, A. M. Asiri, Q. Van Le, V.-H. Nguyen and P. Singh, Covalent organic frameworks promoted single metal atom catalysis: Strategies and applications, *Coord. Chem. Rev.*, 2022, **452**, 214298.

20 S.-Y. Ding, J. Gao, Q. Wang, Y. Zhang, W.-G. Song, C.-Y. Su and W. Wang, Construction of Covalent Organic Framework for Catalysis: Pd/COF-LZU1 in Suzuki–Miyaura Coupling Reaction, *J. Am. Chem. Soc.*, 2011, **133**, 19816–19822.

21 P. Dong, Y. Wang, A. Zhang, T. Cheng, X. Xi and J. Zhang, Platinum Single Atoms Anchored on a Covalent Organic Framework: Boosting Active Sites for Photocatalytic Hydrogen Evolution, *ACS Catal.*, 2021, **11**, 13266–13279.

22 X. Li, C. Zhang, M. Luo, Q. Yao and Z.-H. Lu, Ultrafine Rh nanoparticles confined by nitrogen-rich covalent organic frameworks for methanolysis of ammonia borane, *Inorg. Chem. Front.*, 2020, **7**, 1298–1306.

23 G.-J. Chen, X.-B. Li, C.-C. Zhao, H.-C. Ma, J.-L. Kan, Y.-B. Xin, C.-X. Chen and Y.-B. Dong, Ru Nanoparticles-Loaded Covalent Organic Framework for Solvent-Free One-Pot Tandem Reactions in Air, *Inorg. Chem.*, 2018, **57**, 2678–2685.

24 B. Shahzad, Y. Li, D. Xinfang, Y. Ding, Z. Xu, M. K. Zaman, R. M. Irfan and C. Huang, Reconstruction of nitrogen-containing covalent organic framework-coordinated Ir single-atom electrocatalysts for high-performance lithium-rich oxygen battery cathodes, *J. Mater. Chem. C*, 2023, **11**, 7817–7824.

25 Z. Zheng, Z. Li, Y. Yang, X. Wang, S. Wang, Z. Zhang, T. Kang, X. Chen, W.-J. Wang, Y. Ding, P. Braunstein and P. Liu, Surface deposition of 2D covalent organic frameworks for minimizing nanocatalyst sintering during hydrogenation, *Chem. Commun.*, 2022, **58**, 10016–10019.

26 D. Mullangi, D. Chakraborty, A. Pradeep, V. Koshti, C. P. Vinod, S. Panja, S. Nair and R. Vaidhyanathan, Highly Stable COF-Supported Co/$Co(OH)_2$ Nanoparticles Heterogeneous Catalyst for Reduction of Nitrile/Nitro Compounds under Mild Conditions, *Small*, 2018, **14**, 1801233.

27 X. Ren, C. Li, J. Liu, H. Li, L. Bing, S. Bai, G. Xue, Y. Shen and Q. Yang, The Fabrication of Pd Single Atoms/Clusters on COF Layers as Co-catalysts for Photocatalytic H_2 Evolution, *ACS Appl. Mater. Interfaces*, 2022, **14**, 6885–6893.

28 C.-T. Kuo, Y. Lu, P. Arab, K. S. Weeraratne, H. El-Kaderi and A. M. Karim, 18.1% single palladium atom catalysts on mesoporous covalent organic framework for gas phase hydrogenation of ethylene, *Cell Rep. Phys. Sci.*, 2021, **2**, 100495.

29 M. Economidou, N. Mistry, K. M. P. Wheelhouse and D. M. Lindsay, Palladium Extraction Following Metal-Catalyzed Reactions: Recent Advances and Applications in the Pharmaceutical Industry, *Org. Process Res. Dev.*, 2023, **27**, 1585–1615.

30 Q. Li, R. Zhao, Z. Lu, L. Xiao and L. Hou, Energy transfer photocatalyst enabled by covalent organic framework induced reversible complexation-mediated polymerization under white LED light irradiation and the mechanism study, *Mater. Today Chem.*, 2022, **26**, 101253.

Open Access Article. Published on 16 December 2025. Downloaded on 2/14/2026 6:47:07 PM. This article is licensed under a Creative Commons Attribution-NonCommercial 3.0 Unported Licence.

31 B. Zhang, H. Liu, P. Zhai, R. Zhang, W. Wang, P. Khangale, D. Hildebrandt, X. Liu and S. Qiao, Well-Defined Conjugated Reticular Oligomer "Blood Cells" and Conducting Polymer "Neurons" Constructing "Muscle"-Biomimetic Electrocatalysts for Water Electrolysis, *Adv. Funct. Mater.*, 2023, **33**, 2211440.

32 H. Yang, Z. Lu, X. Yin, S. Wu and L. Hou, Influence laws of air gap structure manipulation of covalent organic frameworks on dielectric properties and exciton effects for photopolymerization, *Chem. Sci.*, 2023, **14**, 8095–8102.

33 J.-M. Seo, H.-J. Noh, H. Y. Jeong and J.-B. Baek, Converting Unstable Imine-Linked Network into Stable Aromatic Benzoxazole-Linked One via Post-oxidative Cyclization, *J. Am. Chem. Soc.*, 2019, **141**, 11786–11790.

34 S. Abi Fayssal, T. Naret, J. Buendia, A. Labattut, V. Huc, C. Martini and E. Schulz, Synthesis, Catalytic Activity and Comparative Leaching Studies of Calix[8]arene-Supported Pd-NHC Complexes for Suzuki-Miyaura Cross-Couplings, *Adv. Synth. Catal.*, 2022, **364**, 947–957.

35 P. Soares, C. Fernandes, D. Chavarria and F. Borges, Microwave-Assisted Synthesis of 5-Phenyl-2-hydroxyacetophenone Derivatives by a Green Suzuki Coupling Reaction, *J. Chem. Educ.*, 2015, **92**, 575–578.

36 M. Allegretti, V. Berdini, M. C. Cesta, R. Curti, L. Nicolini and A. Topai, One-pot, new stereoselective synthesis of endo-tropanamine, *Tetrahedron Lett.*, 2001, **42**, 4257–4259.

37 P. Mauleón, I. Alonso and J. C. Carretero, Unusual Palladium-Catalyzed Cascade Arylation of α,β-Unsaturated Phenyl Sulfones under Heck Reaction Conditions, *Angew. Chem., Int. Ed.*, 2001, **40**, 1291–1293.

38 M. Thommes, K. Kaneko, A. V. Neimark, J. P. Olivier, F. Rodriguez-Reinoso, J. Rouquerol and K. S. W. Sing, Physisorption of gases, with special reference to the evaluation of surface area and pore size distribution (IUPAC Technical Report), *Pure Appl. Chem.*, 2015, **87**, 1051–1069.

39 C. Kang, Z. Zhang, V. Wee, A. K. Usadi, D. C. Calabro, L. S. Baugh, S. Wang, Y. Wang and D. Zhao, Interlayer Shifting in Two-Dimensional Covalent Organic Frameworks, *J. Am. Chem. Soc.*, 2020, **142**, 12995–13002.

40 Ü. Yilmaz, H. Küçükbay, S. Türktekin Çelikesir, M. Akkurt and O. Büyükgüngör, Synthesis of novel benzimidazole salts and microwave-assisted catalytic activity of in situ generated Pd nanoparticles from a catalyst system consisting of benzimidazol salt, $Pd(OAc)_2$, and base in a Suzuki-Miyaura reaction, *Turk. J. Chem.*, 2013, **37**, 721–733.

41 L. Xu, X.-C. Wu and J.-J. Zhu, Green preparation and catalytic application of Pd nanoparticles, *Nanotechnology*, 2008, **19**, 305603.

42 R. Molaei, K. Farhadi, M. Forough and S. Hajizadeh, Green Biological Fabrication and Characterization of Highly Monodisperse Palladium Nanoparticles Using Pistacia Atlantica Fruit Broth, *J. Nanostruct.*, 2018, **8**, 47–54.

43 T. Borkowski, A. M. Trzeciak, W. Bukowski, A. Bukowska, W. Tylus and L. Kępiński, Palladium(0) nanoparticles formed in situ in the Suzuki–Miyaura reaction: The effect of a palladium(II) precursor, *Appl. Catal., A*, 2010, **378**, 83–89.

44 T. Zahra, K. S. Ahmad, C. Zequine, R. Gupta, A. Thomas, M. A. Malik, S. Iram and D. Ali, Biomimmetic ZrO@PdO nanocomposites: fabrication, characterization, and water splitting potential exploration, *Int. J. Energy Res.*, 2022, **46**, 8516–8526.

45 T. Pillo, R. Zimmermann, P. Steiner and S. Hüfner, The electronic structure of PdO found by photoemission (UPS and XPS) and inverse photoemission (BIS), *J. Phys.: Condens. Matter*, 1997, **9**, 3987.

46 H. Borchert, B. Jurgens, V. Zielasek, G. Rupprechter, S. Giorgio, C. Henry and M. Baumer, Pd nanoparticles with highly defined structure on MgO as model catalysts: An FTIR study of the interaction with CO, O_2, and H_2 under ambient conditions, *J. Catal.*, 2007, **247**, 145–154.

47 A. I. Boronin, E. M. Slavinskaya, I. G. Danilova, R. V. Gulyaev, Yu. I. Amosov, P. A. Kuznetsov, I. A. Polukhina, S. V. Koscheev, V. I. Zaikovskii and A. S. Noskov, Investigation of palladium interaction with cerium oxide and its state in catalysts for low-temperature CO oxidation, *Catal. Today*, 2009, **144**, 201–211.

48 F. Di Gregorio, L. Bisson, T. Armaroli, C. Verdon, L. Lemaitre and C. Thomazeau, Characterization of well faceted palladium nanoparticles supported on alumina by transmission electron microscopy and FT-IR spectroscopy of CO adsorption, *Appl. Catal., A*, 2009, **352**, 50–60.

49 Y. Pérez, M. L. Ruiz-González, J. M. González-Calbet, P. Concepción, M. Boronat and A. Corma, Shape-dependent catalytic activity of palladium nanoparticles embedded in SiO_2 and TiO_2, *Catal. Today*, 2012, **180**, 59–67.

50 H. Wang and C. Liu, Preparation and characterization of SBA-15 supported Pd catalyst for CO oxidation, *Appl. Catal., B*, 2011, **106**, 672–680.

51 P. S. Cremer, X. Su, Y. R. Shen and G. A. Somorjai, Ethylene Hydrogenation on Pt(111) Monitored in Situ at High Pressures Using Sum Frequency Generation, *J. Am. Chem. Soc.*, 1996, **118**, 2942–2949.

52 F. Zaera, On the Mechanism for the Hydrogenation of Olefins on Transition-Metal Surfaces: The Chemistry of Ethylene on Pt(111), *Langmuir*, 1996, **12**, 88–94.

53 A. M. Argo, J. F. Odzak, J. F. Goellner, F. S. Lai, F.-S. Xiao and B. C. Gates, Catalysis by Oxide-Supported Clusters of Iridium and Rhodium: Hydrogenation of Ethene, Propene, and Toluene, *J. Phys. Chem. B*, 2006, **110**, 1775–1786.

54 C. Bianchini, E. Farnetti, M. Graziani, J. Kaspar and F. Vizza, Molecular solid-state organometallic chemistry of tripodal (polyphosphine)metal complexes. Catalytic hydrogenation of ethylene at iridium, *J. Am. Chem. Soc.*, 1993, **115**, 1753–1759.

55 A. Uzun and B. C. Gates, Dynamic Structural Changes in a Molecular Zeolite-Supported Iridium Catalyst for Ethene Hydrogenation, *J. Am. Chem. Soc.*, 2009, **131**, 15887–15894.

56 V. Bernales, D. Yang, J. Yu, G. Gümüşlü, C. J. Cramer, B. C. Gates and L. Gagliardi, Molecular Rhodium Complexes Supported on the Metal-Oxide-Like Nodes of Metal Organic Frameworks and on Zeolite HY: Catalysts for Ethylene Hydrogenation and Dimerization, *ACS Appl. Mater. Interfaces*, 2017, **9**, 33511–33520.

 This journal is © The Royal Society of Chemistry 2026

Open Access Article. Published on 16 December 2025. Downloaded on 2/14/2026 6:47:07 PM.
This article is licensed under a Creative Commons Attribution-NonCommercial 3.0 Unported Licence.

57 E. Guan and B. C. Gates, Stable Rhodium Pair Sites on MgO: Influence of Ligands and Rhodium Nuclearity on Catalysis of Ethylene Hydrogenation and H–D Exchange in the Reaction of H_2 with D_2, *ACS Catal.*, 2018, **8**, 482–487.
58 J. C. Fierro-Gonzalez and B. C. Gates, Catalysis by gold dispersed on supports: the importance of cationic gold, *Chem. Soc. Rev.*, 2008, **37**, 2127–2134.
59 J. Guzman, A mononuclear gold complex catalyst supported on MgO: spectroscopic characterization during ethylene hydrogenation catalysis, *J. Catal.*, 2004, **226**, 111–119.
60 R. D. Cortright, S. A. Goddard, J. E. Rekoske and J. A. Dumesic, Kinetic study of ethylene hydrogenation, *J. Catal.*, 1991, **127**, 342–353.
61 G. Bond and P. Wells, The hydrogenation of acetylene I. The reaction of acetylene with hydrogen catalyzed by alumina-supported platinum, *J. Catal.*, 1965, **4**, 211–219.
62 G. Bond and P. Wells, The hydrogenation of acetylene II. The reaction of acetylene with hydrogen catalyzed by alumina-supported palladium, *J. Catal.*, 1966, **5**, 65–73.
63 J. Moses, A. Weiss, K. Matusek and L. Guczi, The effect of catalyst treatment on the selective hydrogenation of acetylene over palladium/alumina, *J. Catal.*, 1984, **86**, 417–426.
64 L. Z. Gva and K. E. Kho, Kinetics of acetylene hydrogenation on palladium deposited on alumina, *Kinet. Catal.*, 1988, **29**, 381–386.
65 R. B. Moyes, D. W. Walker, P. B. Wells, D. A. Whan and E. A. Irvine, An unusual form of non-Arrhenius behaviour in ethyne hydrogenation over palladium catalysts, *Appl. Catal.*, 1989, **55**, L5–L8.
66 H. R. Aduriz, P. Bodnariuk, M. Dennehy and C. E. Gigola, Activity and selectivity of $Pd/\alpha\text{-}Al_2O_3$ for ethyne hydrogenation in a large excess of ethene and hydrogen, *Appl. Catal., A*, 1990, **58**, 227–239.
67 H. Molero, D. Stacchiola and W. T. Tysoe, The kinetics of ethylene hydrogenation catalyzed by metallic palladium, *Catal. Lett.*, 2005, **101**, 145–149.
68 E. Guan, L. Debefve, M. Vasiliu, S. Zhang, D. A. Dixon and B. C. Gates, MgO-Supported Iridium Metal Pair-Site Catalysts Are More Active and Resistant to CO Poisoning than Analogous Single-Site Catalysts for Ethylene Hydrogenation and Hydrogen–Deuterium Exchange, *ACS Catal.*, 2019, **9**, 9545–9553.
69 C. Schöttle, E. Guan, A. Okrut, N. A. Grosso-Giordano, A. Palermo, A. Solovyov, B. C. Gates and A. Katz, Bulky Calixarene Ligands Stabilize Supported Iridium Pair-Site Catalysts, *J. Am. Chem. Soc.*, 2019, **141**, 4010–4015.
70 S. Goddard, Deuterium tracing studies and microkinetic analysis of ethylene hydrogenation over platinum, *J. Catal.*, 1992, **137**, 186–198.